Accuracy Evaluation and Exploration of Measurement Uncertainty for Exact Helical Cone Beam Reconstruction Using Katsevich Filtered Backprojection in Comparison to Circular Feldkamp Reconstruction with Respect to Industrial CT Metrology

Jens MUDERS*, Jürgen HESSER*, Andreas LACHNER**, Christof REINHART**
* Experimental Radiation Oncology - University Medical Center Mannheim
(Theodor-Kutzer-Ufer 1-3, 68167 Mannheim, jmuders@gmail.com)
** Volume Graphics GmbH
(Wieblinger Weg 92a, 69123 Heidelberg, lachner@volumegraphics.com)

Abstract. New requirements to scan long objects are fostering the use of helical scan trajectories. An exact filtered backprojection-based method has been suggested by Katsevich. In this paper, we investigate the applicability of this reconstruction strategy in industrial CT vs. conventional filtered backprojection type reconstructions. Hereby, we study the accuracy and the measurement uncertainty in terms of length and form deviations by using a circular and helical scans of a calibrated cube with spherical caps. The results show that Katsevich's helical algorithm can theoretically lead to more accurate measurements than circular FDK, but that it requires a more precise calibration during data acquisition.

1. Introduction

In industrial CT (ICT) metrology, accuracy and reliability of measurement are vitally important, but influenced by many factors. An important influence is the choice of scanning geometry and applied reconstruction algorithm. With a circular scanning path, the *Feldkamp-Davis-Kress* (FDK) algorithm [1] is often used. For scans based on a helical trajectory, *Katsevich* proposed an exact filtered backprojection (FBP) algorithm [2,3].

Both techniques require certain sets of geometric and algorithmic parameters to work correctly and to achieve minimal measurement errors. Despite the fact that for FDK the crucial parameters have been studied intensively so far, circular scans produce artifacts, especially at the top and bottom of the scanned object, because the amount of data acquired there is not sufficient for an artifact-free reconstruction [4].

In contrast to this, *Katsevich's* algorithm allows reconstructing an object without introducing artifacts at the axial borders of the object. Although the approach is considered to deliver more accurate results than standard FDK, it depends on the type of implementation and on the choice of parameters. Up to now, the exact helical FBP is not frequently used in ICT metrology and only few studies have been conducted on real data [5,6]. However, to use the algorithm for dimensional measurements it needs to be well tested with respect to reliable results.

License: http://creativecommons.org/licenses/by/3.0/

Therefore, the aim of this paper is to explore measurement uncertainty of *Katsevich's* helical reconstruction in comparison to the FDK algorithm by analyzing and calibrating the parameters that influence the image quality of the reconstructed object. Our study will be performed on simulated and real data comparing circular and helical scans of a cube with spherical caps on three sides by applying coordinate measurement templates using *VGStudio MAX* to identify deviations in the gray values and the shape of the reconstructed results. By tuning parameters, the exactness of the performed measurements using *Katsevich's* algorithm on a helical scanning path will be quantified in relation to circular scans using FDK. As a result, the examination will approve the expected measurement uncertainty and outline the limitations of both techniques with respect to industrial CT.

This paper is organized as follows. In Section 2 we give an overview of the scanning systems and the parameters used to acquire our data. Afterwards we describe both reconstruction algorithms and the methods used to evaluate and to compare the circular and helical scans. The detailed results of this evaluation are given in Section 3. Finally, in Section 4 we discuss the results in the context of measurement uncertainty.

2. Material and Methods

1.1 Data acquisition

The object of interest used in our evaluative study is a cube made of titan alloy manufactured by *FEINMESS GmbH & Co. KG*. The cube has a size of 10×10×10 mm³ and 25 equidistantly spaced spherical caps on three sides with each having a radius of 0.4±0.0008 mm. The lengths and the position of the caps have been calibrated by *Deutscher Kalibrierdienst* (DKD) using tactile measurements.

Table 1. Technical specifications of the used CT scanner.

CT scanner: v|tome|x s 225			
Manufacturer	Phoenix x-ray (GE Sensing & Inspection Technologies)	Detector	Perkin Elmer 840
		Detector area	204.8 × 204.8 mm²
X-ray tube	Microfocus	Pixel number	512 × 512
Max. tube voltage	225 kV	Pixel Pitch	400 µm
Max. output	320 W	Dist. Source-Object	68.5492 mm
		Dist. Source-Detector	783.4191 mm

The data that we acquired from this calibrated cube has been scanned by a *phoenix x-ray v|tome|x s 225* industrial cone beam CT scanner at the *TPW Prüfzentrum* in Neuss. The technical specifications of the scanner are depicted in Table 1. The *v|tome|x s 225* is a high-resolution system that can be configured in a macro-based fashion to run scans with various scanning trajectories. In our case the scanner was used to perform three scans using the distances (source-to-object and source-to-detector) as described in Table 1. The first scan in this sequence was carried out on a circular trajectory while capturing 2000 projections over an angular range of 360 degree. After this scan the system was configured to acquire 2000 projections on a helical trajectory over an angular range of 720 degree (2 turns). Finally, the scanner made another helical scan collecting 1000 projections over 360 degree (1 turn). For last two scans we used a total helical pitch of 25.0 mm. As shown in Table 2 another scan has been added to the evaluation by leaving out every second projection of the first scan, leading to four different acquisition schemes. The scanning parameters for all four setups are summarized in Table 2.

Table 2. Four different settings of parameters defining scanning and reconstruction geometries.

Trajectory	Number of Projections	Angular Range [degree]	Pitch [mm]
Circular	2000	360.0	0.0
Helical	2000	720.0	12.5
Helical	1000	360.0	25.0
Circular	1000	360.0	0.0
Volume size	512 × 512 × 512		
Voxel size	35 µm		

In addition to the real data from the *phoenix x-ray v|tome|x s 225*, we generated simulated projection data to verify the correctness of our implemented reconstruction algorithms and to demonstrate the theoretical optimum of our evaluation. To simulate projections of the volume of interest we used our own implementation of a sampling based ray casting method, following the one presented in [7]. Although the simulation is carried out on a single precision GPU using *NVDIA's CUDA Toolkit 3.2* the accuracy of the projection data has been improved by setting the sampling rate along the ray twice as high as the sampling rate of the volume, by using higher order integration [8] and by the application of the *Kathan* summation algorithm [9].

1.2 Reconstruction algorithms

For the reconstruction of the volume datasets from the real and from the simulated projections within *VGStudio MAX*, we used a volume size of 512×512×512 voxels with a sampling distance of 35 µm. The circular scans were reconstructed using the FDK algorithm [1] for cone beam filtered backprojection. For the filtration part of this algorithm the *Shepp-Logan* filter was selected and from the sinogram of the real projection data a horizontal detector offset of -0.6063 mm was estimated. The simulated datasets of the circular and of the helical setups were processed without any detector offsets.

In contrast to the circular case, the projections acquired from the helical scans were reconstructed using the theoretical exact filtered backprojection algorithm for helical cone beam proposed by *Katsevich* [2]. Our implementation follows the ones proposed in [10-14]. First the derivatives of the cone beam projections at constant directions along the source trajectory are computed by using 2-point differences [10]. Then the projections are rebinned to tilted lines on the detector using bilinear interpolation, followed by a Hilbert transform implemented by FFT [12]. Afterwards a backward rebinning step interpolates the tilted projections to the original detector coordinates [11]. The final backprojection step is preceded by a weighting of the filtered projection data [13] according to the cone beam cover method proposed in [14]. Finally, each projection is backprojected using a voxel driven approach that can be either executed on the CPU or on the GPU using CUDA.

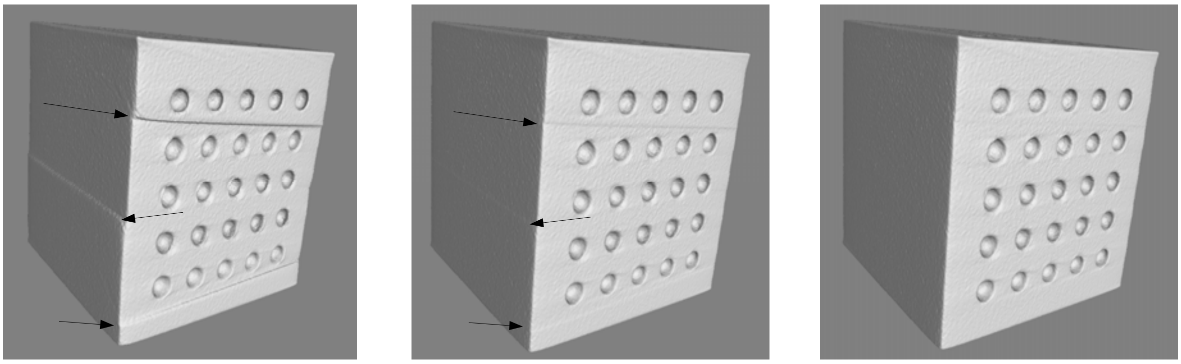

Figure 1. Comparison of different choices for the horizontal detector offset during helical reconstruction from real data. A choice of 0.0 mm (left) and of -0.6 mm as in the circular case (middle) introduced step artifacts in the reconstructed volume. Manually tuning the parameter for the detector offset to -0.76 mm yielded the best results (right).

Similar to the circular scans a horizontal detector offset had to be determined for the helical scans. Although the circular and the helical setups for the scanner were the same, the determined detector offsets were not equal. The horizontal offset for the helical case had to be manually tuned to yield reasonable reconstructions. Figure 1 show the reconstructed volumes of the helical scan (2000 projections) with different values for the parameter of the horizontal detector offset. When setting the parameter to 0.0 mm or to the same value as in the circular FDK reconstruction (-0.6 mm) step artifacts occurred in the final volume (see left and middle image of Figure 1). A manually determined value of -0.76 mm for the horizontal detector offset yielded the best results in both helical scans.

1.3 Evaluation methods

For the evaluation of the acquired data and the comparison of the two reconstruction algorithms we started by looking at the gray value and noise properties by computing the signal-to-noise ratio (SNR) of the reconstructed volume from the mean of the signal μ_{sig} divided by the standard deviation of the background σ_{bg}.

After this we used *VGStudio MAX* to determine the exactness of the reconstructions in terms of measurement uncertainty. By using a predefined measurement template, that contained all the features of the cube and its spherical caps, it was possible to apply the evaluation equally to all reconstructed volumes. Because of this, the following steps were used to evaluate each reconstructed dataset:

1. Reconstruction of the cube using the cone beam FDK for data from circular and the exact spiral FBP for data from helical trajectories.
2. With the volume inside *VGStudio MAX* an "Advanced Surface Determination" has been computed to define the surface of the cube and to use the registration functionalities of *VGStudio MAX*.
3. Then we merged the predefined measurement template into the scene and fitted the volume and the template by hand, so that their boundaries roughly aligned.
4. By copying and pasting the measurement template to the manually aligned volume the reference objects (spheres) of the template were fit to the spherical caps of the reconstructed cube.
5. To improve the alignment of the volume with the template we registered the fitted reference objects of the volume with the reference objects of the imported measurement template.
6. Then we deleted the fitted measurements at the volume and repeated step 4 to improve the fitting of the reference objects (spheres).
7. Finally, we adjusted the resolution of the reconstructed volume using nine within the template predefined features which measure the actual lengths between some of the spheres. The nominal lengths of these features were computed from the DKD calibration certificate. In an iterative process the resolution of the volume was corrected, so that the actual lengths of the features fitted their nominal values.

After all these steps the measurement template with its reference objects fitted the reconstructed cube and the template was used to compute the center and the surface form of each spherical cap. We then used the position of the spheres to compute deviations of the actual lengths from their nominal values. Additionally the surface form, which is defined by the sum of the profile peak height Z_p and the profile valley depth Z_v [15], quantifies the amount of distortion introduced by the scanning geometry and by the used reconstruction algorithm.

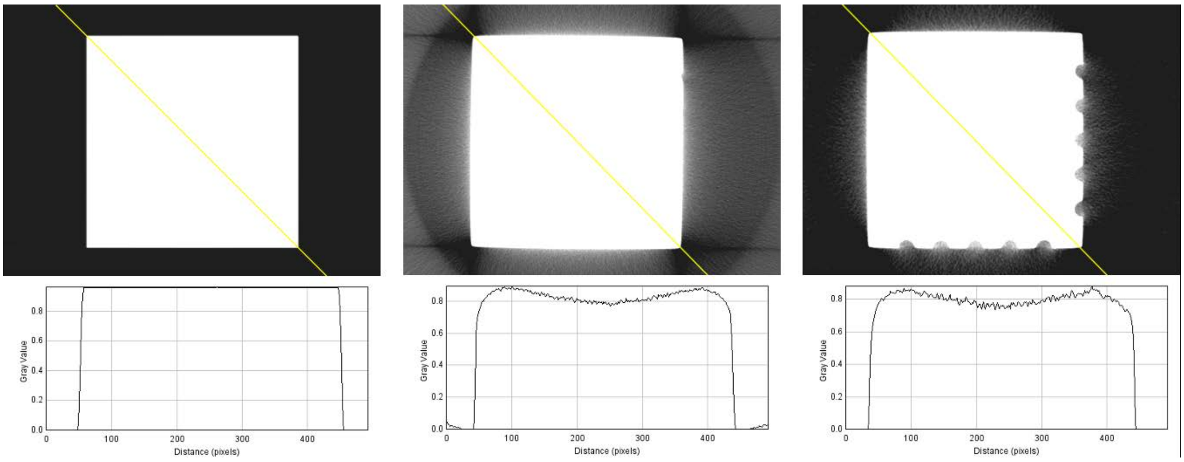

Figure 3. Central axial slices of the reconstructed cube (window = 0.4, level = 0.15). The left image shows the reconstruction from the simulated helical projections. The middle image and the right image show the cube reconstructed from real data. The profiles below the slices show the gray value profiles along the yellow line in the slice images.

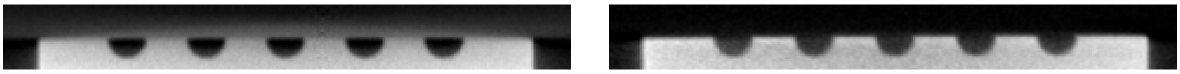

Figure 2. Artifacts at the top of the reconstructed cube. In the FDK reconstructed object (left) cone beam artifacts occur at the top of the cube. When using the Katsevich's FBP algorithm no cone beam artifacts are visible (right).

3. Evaluation

3.1 Noise Statistics and Grey Value

Comparing the noise characteristics of the two reconstruction techniques revealed that in our case the *Katsevich's* FBP algorithm has a better image quality with respect to noise than the FDK algorithm (see Table 3). The signal-to-noise ratio for the FDK with 2000 projections was about 16.79 with only a slightly smaller value when the number of projections was reduced to 1000. In the helical case the signal-to-noise ratio was 23.31 when 2000 projections were used, where a minimal increase could be detected when the number of projections was reduced.

Table 3. Gray value statistics (mean of the signal and standard deviation of the background) and signal to noise ratio of the real datasets.

Traj.	**Proj.**	μ_{sig}	σ_{bg}	**SNR**
Circ.	1000	0,8161	±0,0490	16,6716
Circ.	2000	0,8312	±0,0495	16,7910
Hel.	1000	0,7875	±0,0335	23,5189
Hel.	2000	0,8075	±0,0346	23,3181

When considering the grey values for the circular FDK reconstructions and for the reconstructions using *Katsevich's* FBP algorithm, it can be seen that the corners of the cube are undersampled in the real datasets, while in the simulated dataset the corners of the cube show no sampling artifacts (see Figure 2). Due to this drop-off at the corners in the real datasets of both circular and helical reconstructions the sides of the cube appear slightly bended. This artifact could be due to scattering effects, because in the reconstructions from the simulated datasets the sides are perfectly flat.

Another artifact that occurs only in the circular FDK reconstruction is shown in Figure 3. Looking at the cube from the side the top and bottom of the object show so-called *Feldkamp* artifacts (see Figure 3) due to the circular scanning geometry [4].

3.1 Length Deviation

To quantify and to compare the accuracy of the reconstructions and to make statements about the measurement uncertainty the differences between the actual and the nominal distances of all spherical caps to each other are computed for the real and simulated datasets. Table 4 shows the resulting mean and standard deviation of the absolute differences for three different combinations of the spherical caps. In the left column ("All panes") the distances between all 75 spherical caps have been include in the computation. The results show that in the circular reconstructions the mean of the absolute length deviation is between 9 and 10 µm, what is about one third of the actual voxel size of 35 µm. The length deviation of 10.4 µm for the reconstruction from the simulated projections can be seen as a rough theoretical lower bound for the circular cases. Looking at the real data this bound is met by the FDK algorithm showing even lower results (9.1 and 9.0 µm). In contrast to this, the resulting length deviations of the reconstructions using *Katsevich's* helical FBP are higher in the case of real data. In contrast to this, the mean length deviation of 5.7 µm, which is about one sixth of the voxel size, for the simulated helical projections is even lower than in any of the FDK reconstructions.

Table 4. Differences of the actual and the nominal distances between the spherical caps to each other [µm].

Traj.	Data	Proj.	All planes		Plane 1 only		Plane 1 to 2 and 3	
			µ	Σ	µ	σ	µ	σ
Circ.	Real	1000	9.1	±8.4	2.5	±1.9	11.6	±7.6
Circ.	Real	2000	9.0	±8.4	2.6	±2.0	11.5	±7.6
Circ.	Sim.	2000	10.4	±9.3	3.5	±4.2	17.9	±8.1
Hel.	Real	1000	10.9	±9.4	2.6	±2.1	12.4	±9.3
Hel.	Real	2000	10.6	±8.5	5.2	±3.3	11.4	±8.3
Hel.	Sim.	2000	5.7	±5.2	2.3	±3.8	7.8	±5.2

The second column of Table 4 shows the length deviations of the 25 spherical caps that lie on the top plane of the cube. The results show significantly lower values (2.3 to 5.2 µm) as the ones from the previous column, but the circular reconstructions still outperform the helical datasets with only one exception: the measurements on the simulated helical data show the lowest mean value of 2.3 µm.

In the third column only the distances between the caps on top and the caps on the two other sides contribute to the computed length deviations. The lengths between the caps of the same plane and between caps of the two side planes have been excluded from these calculations. The results for all scans show slightly higher values (11.4 to 17.9 µm) as when considering all distances between all spherical caps (first column). In comparison to the first two columns, the reconstructions from the real data with 2000 projections deliver almost similar length deviations (11.4 µm in the helical and 11.5 µm in the circular case). As in two previous columns a theoretical lower bound (of 7.8 µm) is given by the

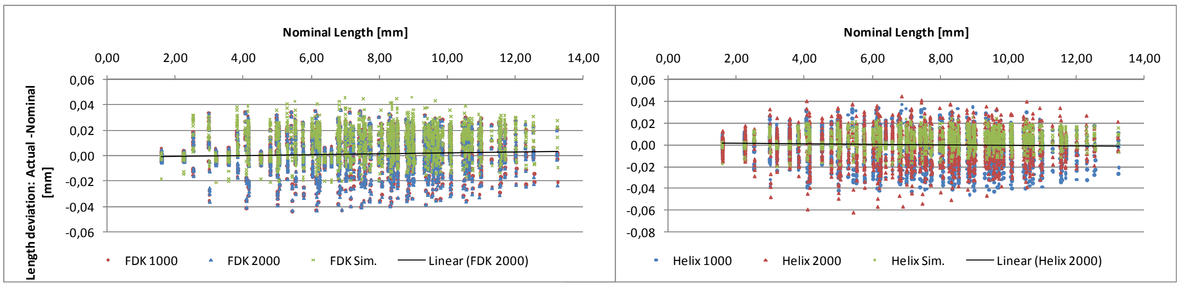

Figure 4. Deviations between the actual and the nominal distances between the spherical caps of the cube. The length deviations for all circular (left) and helical (right) reconstructions are plotted against their calibrated nominal lengths. For the reconstructions from the 2000 real projections a linear trend line has been fitted to the datasets.

reconstruction from the simulated helical data and is not reached by any real dataset.

A comparison between the length deviation and the corresponding nominal length shows that our circular reconstructions using the FDK algorithm with 2000 and 1000 projections deliver almost the same results independent of the nominal length. In contrast to this the simulated dataset shows a positive bias in its length deviation (see left image of Figure 4). In the two helical reconstructions with 2000 and with 1000 projections the length deviations distribute quite similar like in the circular case (see right image of Figure 5), but the reconstruction from the simulated projections shows no bias in its length deviations and has a smaller range (-20 to 20 µm) as the reconstruction from the simulated circular data.

3.2 Form Deviation

Additionally to the length deviations, the differences between the actual and the nominal surface form (Z_p+Z_v) of the spherical caps have been computed and averaged over all planes and over every single plane (Table 5). The mean form deviations of the real datasets presented in Table 4 range from 10.1 µm (about one third of the voxel size) for the circular scan at 2000 projections up to 21.5 µm for the helical scans. Comparing the form factors of the circular trajectory with the ones from the helical trajectory shows that the measurements on the circular cases are up to a factor of 2 more accurate. The calculated surface form deviations for the reconstructions from the simulated projections are always lower than the ones from the real datasets. When comparing the single planes of the cube, no plane shows large deviations from the overall mean of the surface form (first column).

Table 5. Differences between the actual and the nominal surface form of the spherical caps [µm].

Traj.	Data	Proj.	All planes		Plane 1		Plane 2		Plane 3	
			µ	σ	µ	σ	µ	Σ	µ	σ
Circ.	Real	1000	12.2	±5.8	11.5	±5.9	11.8	±5.1	13.5	±6.3
Circ.	Real	2000	10.6	±5.4	10.1	±4.9	10.6	±4.9	11.2	±6.4
Circ.	Sim.	2000	7.7	±6.1	7.8	±7.9	9.8	±3.7	5.6	±5.2
Hel.	Real	1000	17.3	±7.9	14.0	±8.0	19.7	±6.4	18.4	±8.1
Hel.	Real	2000	18.3	±7.7	13.4	±7.5	20.0	±6.9	21.5	±6.4
Hel.	Sim.	2000	9.7	±6.6	12.8	±8.3	10.4	±3.7	6.0	±5.2

4. Discussion and Conclusion

The evaluations in this paper show that on the one hand the reconstructions from the real circular projections delivered better result in terms measurement uncertainty (length deviations and form deviations) even though the helical reconstructions of the cube showed no cone beam artifacts at the upper and lower planes. On the other hand, looking at the reconstructions from the simulated datasets *Katsevich's* helical FBP algorithm results in the smallest length deviations in comparison to all other datasets. This fact suggests that there is a gap between the processing of real and simulated projections and that there is potential to optimize the helical reconstruction algorithm for real datasets.

For example, the lower signal-to-noise ratio in the circular case can be explained by the loss of spatial resolution in the direction of the rotation axis [6] due the unfulfilled *Tuy-Smith* sufficiency condition [16] introducing *Feldkamp* artifacts and thus raising the background noise (see Table 3). Although *Katsevich's* algorithm has lower detector utilization, where only data from inside the *Tam-Danielson* window is used to reconstruct the cube, it shows a higher signal-to-noise ratio. An increase in the detector utilization using a technique that incorporates redundant data from the detector into an exact helical reconstruction [17,18] would not only increase the signal-to-noise ratio for the helical cases even further, but could also influence the accuracy of measurements positively.

Considering the length and form deviations it must be kept in mind that for the circular reconstructions we were able to extract the detector offset from the sinogram, whereas in the helical datasets we determined it manually. This in combination with the fact that all helical reconstructions, including *Katsevich's* algorithm, depend on an additional shift in the axial direction demonstrates that a larger number of parameters are influencing the reconstruction and thus providing more space for measurement errors. In our case, when fine tuning the parameters for the detector offset and for the helical pitch we got varying results for the length and form deviations.

In summary, even if *Kasevich's* algorithm shows best results on simulated data, our study demonstrated that in the case of real data the influence and the uncertainty of geometric parameters make a precise calibration of the CT scanner necessary to increase the accuracy of helical acquisitions and reconstructions.

References

[1] L. Feldkamp, L. Davis, and J. Kress, “Practical cone-beam algorithm,” *JOSA A*, vol. 1, Jun. 1984, p. 612–619.

[2] A. Katsevich, “Theoretically exact filtered backprojection-type inversion algorithm for spiral CT,” *SIAM Journal on Applied Mathematics*, vol. 62, 2002, p. 2012–2026.

[3] A. Katsevich, “An improved exact filtered backprojection algorithm for spiral computed tomography,” *Advances in Applied Mathematics*, vol. 32, May. 2004, p. 681–697.

[4] J.F. Barrett and N. Keat, “Artifacts in CT: Recognition and Avoidance,” *Radiographics*, vol. 24, 2004, p. 1679.

[5] T. Schön, I. Bauscher, T. Fuchs, U. Hassler, J. Hiller, and S. Kasperl, “Dimensionelles Messen mit Helix-Computertomographie,” 2009, pp. 1-2.

[6] J. Hiller, S. Kasperl, T. Schön, S. Schröpfer, and D. Weiss, “Comparison of Probing Error in Dimensional Measurement by Means of 3D Computed Tomography with Circular and Helical Sampling,” *ndt.net*, 2010, pp. 1-7.

[7] A. Weinlich, B. Keck, H. Scherl, M. Kowarschik, and J. Hornegger, “Comparison of High-speed ray casting on GPU using CUDA and OpenGL,” *High performance and hardware aware computing*, KIT Scientific Publishing, 2008, p. 25.

[8] M.W. de Boer, A. Gröpl, J. Hesser, and R. Männer, “Reducing artifacts in volume rendering by higher order integration,” *IEEE Visualization’97 Late Breaking Hot Topics*, 1997, p. 1–4.

[9] W. Kahan, “Pracniques: further remarks on reducing truncation errors,” *Communications of the ACM*, vol. 8, 1965, p. 40.

[10] H. Yu and G. Wang, “Studies on implementation of the Katsevich algorithm for spiral cone-beam CT,” *Journal of X-ray Science and Technology*, vol. 12, 2004, p. 97–116.

[11] F. Noo, J. Pack, and D. Heuscher, “Exact helical reconstruction using native cone-beam geometries,” *Physics in Medicine and Biology*, vol. 48, 2003, p. 3787.

[12] A. Wunderlich, “The Katsevich Inversion Formula for Cone-Beam Computed Tomography,” 2006.

[13] G. Yan, J. Tian, S. Zhu, C. Qin, Y. Dai, F. Yang, and P. Wu, “Fast Katsevich algorithm based on GPU for helical cone-beam computed tomography,” *Information Technology in Biomedicine, IEEE Transactions on*, vol. 14, 2010, p. 1053–1061.

[14] J. Yang, Q. Kong, and T. Zhou, “Cone beam cover method: An approach to performing backprojection in Katsevich’s exact algorithm for spiral cone beam CT,” *Journal of X-ray Science and*, 2004, pp. 1-19.

[15] G.T. Smith, *Industrial Metrology*, Springer, 2002.

[16] H.K. Tuy, “An inversion formula for cone-beam reconstruction,” *SIAM Journal on Applied Mathematics*, vol. 43, 1983, p. 546–552.

[17] A. Katsevich, “3PI algorithms for helical computer tomography,” *Advances in Applied Mathematics*, vol. 36, Mar. 2006, p. 213–250.

[18] H. Schöndube, K. Stierstorfer, and F. Noo, “Accurate helical cone-beam CT reconstruction with redundant data,” *Physics in medicine and biology*, vol. 54, 2009, p. 4625.